# Numerical investigation of frequency-amplitude effects of dynamic morphing for a high-lift configuration at high Reynolds number

Abderahmane Marouf, Yannick Bmegaptche Tekap, Nikolaos Simiriotis, Jean-Baptiste Tô, Jean-François Rouchon, Yannick Hoarau, Marianna Braza

# Numerical investigation of frequency-amplitude effects of dynamic morphing for a high-lift configuration at high Reynolds number

Abderahmane MAROUF[*1,2], Yannick BMEGAPTCHE TEKAP[†1], Nikolaos SIMIRIOTIS[‡2], Jean-Baptiste TÔ [§2], Jean-François ROUCHON[¶3], Yannick HOARAU[‖1], and Marianna BRAZA[**2]

[1]ICUBE, University of Strasbourg, France
[2]Institut de Mécanique des Fluides de Toulouse (IMFT), France
[3]Laboratoire Plasma et Conversion d'Energie (LAPLACE), Toulouse, France

## Abstract

**Purpose** - This study illustrates the morphing effects around a large-scale high-lift configuration of the Airbus A320 with two element airfoil-flap in the take-off position. The flow around the airfoil-flap and the near wake are analyzed in the static case and under time-dependent vibration of the flap trailing-edge known as the dynamic morphing.

**Design/methodology/approach** - Experimental results obtained in the subsonic wind tunnel S1 of IMFT of a single wing are discussed with High-Fidelity numerical results obtained by using the NSMB (Navier-Stokes Multiblock) code with advanced turbulent modelling able to capture the predominant instabilities and coherent structure dynamics. An explanation of the dynamic time-dependent grid deformation is provided, which is used in the NSMB code to simulate the flap's trailing-edge deformation in the morphing configuration. Finally, Power Spectral Density is performed to reveal the coherent wake structures and their modification due to the morphing.

**Finding** - Frequency of vibration and amplitude of deformation effects are investigated for different morphing cases. Optimal morphing regions at a specific frequency and a slight deformation were able to attenuate the predominant natural shear-layer frequency

[*]Corresponding Author: amarouf@unistra.fr, abderahmane.marouf@imft.fr
[†]yannick.bmegaptchetekap@imft.fr
[‡]nikolaos.simiriotis@imft.fr
[§]jean-baptiste.to@imft.fr
[¶]rouchon@laplace.univ-tlse.fr
[‖]hoarau@unistra.fr
[**]marianna.braza@imft.fr

and to considerably decrease the width of the von Kármán (vK) vortices with a simultaneous increase of aerodynamic performances.
**Originality/value** - New concept of future morphed wings is proposed for a large scale A320 prototype at the take-off position. The dynamic morphing of the flap's trailing-edge is simulated for a first time for high-lift two-element configuration. In addition, the wake analysis performed helped to show the turbulent structures according to the Organized Eddy Simulation model.
**Paper type** Research paper

## Nomenclature

| | | |
|---|---|---|
| $x/C, z/C$ | = | dimensionless space coordinates |
| $A_m$ | = | amplitude of actuation |
| $C_L$ | = | lift coefficient |
| $C_D$ | = | drag coefficient |
| $f_a$ | = | frequency of actuation |
| $c$ | = | total chord |
| d$t$ | = | time step |
| $\alpha_1$ and $\alpha_2$ | = | angles of attack |
| $Y+$ | = | dimensionless wall distance |
| $CP$ | = | pressure coefficient |
| $Re$ | = | Reynolds number |
| $U$ | = | Velocity magnitude |
| $\omega$ | = | angular velocity |
| $L$ | = | distance between two vortices |
| $\alpha$ and $\beta$ | = | vortex shape parameters |

## 1. Introduction

The aerodynamic design of high-lift configurations needs to fulfil specific targets for take-off and landing configurations. In addition, this system needs to have a minimum complexity of mechanical structure for less weight and cost. Flaps and slats are used to increase aerodynamic performances specially the lift force. During take-off or landing the flap is translated and deflected from its initial position in the airplane. The increase of the wing surface and the camber helps to increase the pressure distribution over it and to improve the lift. A considerable number of studies aimed at investigating the flow around high-lift configurations, as for example in the European project ATAAC http://cfd.mace.manchester.ac.uk/ATAAC/WebHome, where the LEISA three-element wing had been selected and tested experimentally and numerically with a considerable number of CFD codes, involving hybrid RANS-LES turbulence modelling. Synthetic turbulence had been injected in the slat, the flap and the rear part of the wing to predict the flow detachment. The studies of Soulat *et al.* (2016) on shape optimisation for a multi-element device test-case aimed to maximize the lift and minimize the drag.

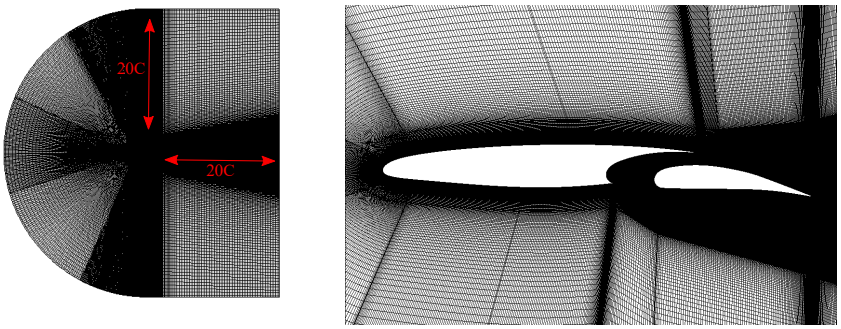


FIGURE 1: Computation grid of the high-lift LS configuration of the A320 in the take-off position

Choosing two different optimizations using only geometrical parameters (geometrical optimization) or the angle of attack and the Mach number (total optimization), they have found for both optimizations quite similar optimal geometric positions : a flap rotation to increase the lift and an upward slat rotation to reduce the drag. In another aerodynamic multi-objective optimization, the study of Lu *et al.* (2017), proposed a flexible variable camber trailing edge of the flap for a two-element airfoil-flap able to camber its shape smoothly at the take-off and landing conditions. They have found that a variable camber of the flap of 50 % of its chord can increase the lift coefficient by about 8 % and the lift-to-drag ratio by 7 % for the take-off configuration and improve the lift coefficient at a stall angle of attack by 1.3 %. A recent study of Abdessemed *et al.* (2018) that proposed to use dynamic meshing to perform numerical simulation of static and time-dependent morphing of a NACA 0012. Their work revealed an increase of the average aerodynamic efficiency CL/CD of 6.5% with a maximum deflection (5 % chord). A considerable number of studies treated shape optimization, static cambering and leading edge with a droop nose aiming at improving aerodynamic performances in order to increase lift, decrease of drag or increase of the stall angle. To our knowledge, there is a lack of experimental and numerical studies investigating a dynamic morphing of a high-lift configuration in respect of the wake dynamics understanding in the high Reynolds number range.

This is the originality of the present study which is part of the H2020 “Smart Morphing and Sensing” (SMS) European project http://smartwing.org/SMS/EU aiming to improve aerodynamic performances as increasing the lift, decreasing the drag and to attenuate the aerodynamic noise by means of novel electroactive morphing concepts. Instead of the classical high-lift system, a morphed flap is installed, able to change its shape dynamically to adapt it to different flight configurations as take-off, cruise and landing. A Multidisciplinary team between Institut de Mécanique des Fluides de Toulouse (IMFT) and Laboratoire Plasma et Conversion d’Energie (LAPLACE) created in 2010 the research platform http://smartwing.org including the participation of six French laboratories in the context of the national research projects EMMAV, DYNAMORPH and SMARTWING followed by a strong collaboration with AIRBUS “Emerging Technologies and Concepts Toulouse” (ETCT) . These activities were supported by the Foundation STAE (Sciences

et Technologies de l'Aéronautique et Espace) http://fondation-stae.net and preceded the European programme SMS, (2017-2020). Chinaud *et al.* (2014) investigated experimentally the electroactive morphing effects obtained by Shape Memory Alloys (SMA) able to considerably bend a flat plate at 10° of incidence and Reynolds number 200,000 at low frequencies (order of 1 Hz). The experiments were carried out by rapid PIV with a sampling rate of 6 KHz. They found that this actuation at low frequency modifies the turbulent structure and the instabilities in the near wake, regarding the von Kármán. Furthermore, an attenuation of the shear-layer amplitude and of the spectral energy is noticed through an increase of the plate's curvature. Afterwards, in the context of the research project DYNAMORPH, Scheller *et al.* (2015) performed an original experimental study of a NACA0012 aileron able to deform and vibrate the near-trailing-edge region thanks to a system of PUSH-PUSH piezoactuators enabling higher-frequency (order of 100 Hz – 300 Hz) low-amplitude deformation. The experiments, using also TRPIV (Time Resolved PIV) revealed the dynamic morphing ability to reduce the Reynolds stress components with a simultaneous significant reduction of the predominant shear layer frequency. The association of low-frequency high-deformation has been the fruit of this multidisciplinary collaboration between the two laboratories IMFT and LAPLACE and reported as "hybrid electroactive morphing", able to operate at different time and length scales of the turbulent motion Chinaud *et al.* (2013). This kind of morphing is partly bio-inspired from the large span hunting birds like the owl, able to simultaneously active their feathers and large wings in order to increase performance and reduce noise, Scheller *et al.* (2015) made an evidence of the hybrid electroactive morphing benefits in the first time in the literature, applied on a NACA4412 morphing wing. These activities had received a high distinction by the Royal Society inviting the multidisciplinary team in its annual exhibition under the theme of "Smart wing design through turbulence control" – Science Imitating Nature" in 2014 in collaboration with Imperial College, London, http://sse.royalsociety.org/2014/smart-wing-design/, followed by the CNRS Journal "the wings of the future" https://lejournal.cnrs.fr/videos/les-ailes-du-futur. Moreover, Jodin *et al.* (2017) constructed an A320 morphing prototype of 70 cm chord, able to camber its rear part beyond 60 % of the chord by an order of 15 % of the whole chord thanks to SMA operating at frequencies less than 1 Hz and simultaneously equipped by MFC (Macro-Fiber Composite) piezo-actuators in the near trailing-edge region, able to vibrate from 30 to 500 Hz, thus ensuring increased capabilities of the hybrid electroactive morphing. They used Time-Resolved PIV (TRPIV) with data acquisition of an order of 6 KHz, pressure and aerodynamic forces measurements at higher-frequency-low-amplitude morphing effect in the trailing edge region and the near wake, as well as the camber control separately and finally the hybrid morphing. It was shown that this association of both classes of actuations is able to produce an order of 3 % more lift, than the only use of the camber control. By means of the Proper Orthogonal Decomposition (POD) and a frequency domain analysis, this study had shown the manipulation of the wake's turbulent structures, a vortex breakdown of the large coherent eddies and enhancement of smaller beneficial eddies thus producing an eddy-blocking effect through shear sheltering process, as explained in Szubert *et al.* (2015) and resulting in thinning the shear layers and the wake's width. This mechanism is fully analyzed for the clean configuration

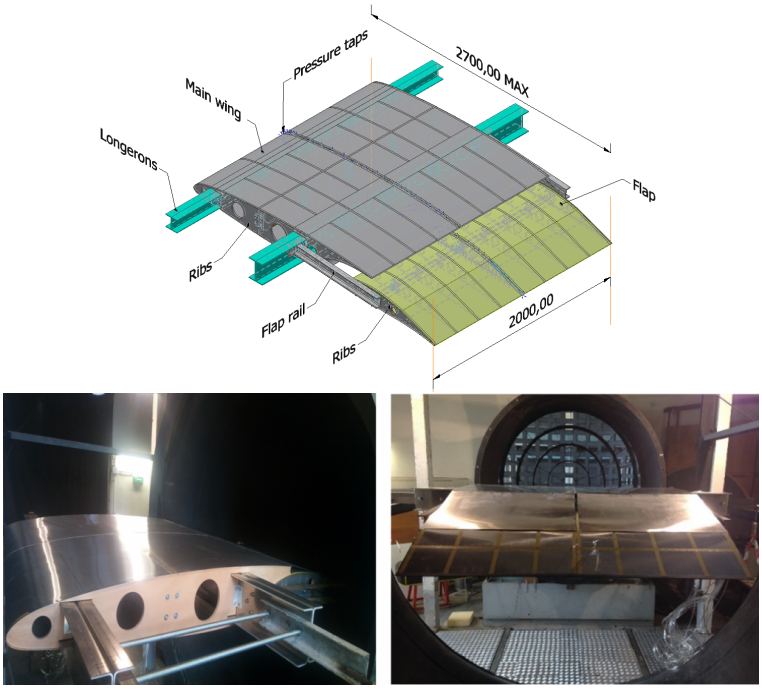


FIGURE 2: The CAD prototype and the experimental high-lift LS prototype mounted in the IMFT wind tunnel

of the present prototype (so-called RS-Reduced Scale prototype of the European project SMS) by numerical simulations and comparisons with the above experiments in our research team in previous studies. A simultaneous lift increase and reduction of the spectral amplitude of predominant peaks corresponding to the shear-layer and wake instabilities were found. The morphing in addition shows a reduction in the noise sources related to the past trailing edge dynamics. Therefore, this hybrid partly bio-inspired morphing has shown experimentally considerable abilities in aerodynamic performances increase.

Our numerical study focuses on the morphing by means of MFC (piezoactuators) near the trailing edge region at low-amplitudes with higher frequencies, applied to a two-element A320 airfoil/flap configuration having a chord of 2.40 m and a flap's chord of 1 m at the take-off position and Reynolds number of $2.25\text{x}10^6$. This corresponds to a near scale 1 configuration of the A320's flap, in the context of the so-called Large Scale (LS) prototype of the European research programme SMS, for which the camber control has been designed experimentally by Jodin *et al.* (2018)

The present numerical study first focuses on the investigation of the morphing effects in the clean configuration of the LS prototype, providing also a validation of the numerical results for this configuration and secondly, the investigation of the morphing effects in the case of the two-element at the take-off configuration (airfoil-gap-flap). The flow dynamics around the A320 airfoil-gap-flap is analysed in detail concerning the static and morphing cases. The shear layer, wake instabilities and dynamics past the airfoil and the flap are dis-

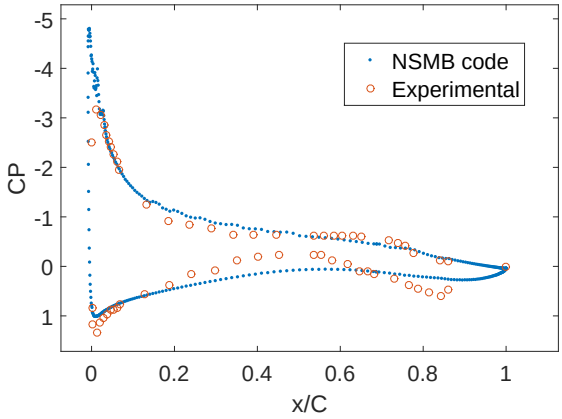


FIGURE 3: Comparison of the mean wall pressure coefficient in the clean configuration of numerical and experimental results : the flap is attached to the wing.

cussed. An explanation of the dynamic morphing is provided regarding the understanding of the modified physical mechanisms when a specific vibration and slight deformation of the flap's trailing edge are added, depending on a fixed actuation frequency. To illustrate the morphing effect over the time-dependent signals of the velocity, spectral analysis of suitably chosen monitor positions was performed and compared with the static case (no vibration) taken as reference case. Finally, the influence of the morphing configuration on the aerodynamic lift and drag coefficients is presented and discussed in relation with the modification of the pressure distribution over the airfoil and the flap due to the morphing. A map of amplitude, frequency and lift coefficient is presented showing the optimal regions of the morphing actuation.

## 2. NUMERICAL AND EXPERIMENTAL CONFIGURATIONS

The numerical flow domain around the airfoil-flap system is considered in this study with farfield boundary conditions at 20 chords from the inlet, outlet, top and bottom as presented in the figure 1. The flap is detached from the airfoil, translated from its initial position and deflected with $10^\circ$ of incidence corresponding to the take-off position for an A320 wing. The resulting total chord of the airfoil and the flap in the take-off is about 2.72 m. The corresponding Reynolds number is around $2.25\text{x}10^6$ and standard air properties have been chosen.

The numerical grid has multiblock structure and it has a CH topology and a size of 0.6 million cells approximately. The mesh has been tested with the numerical solver Navier-Stokes Multi-Block (NSMB), Hoarau *et al.* (2016). This solver is the fruit of a European consortium that included Airbus from the beginning of '90s, as well as the main European aeronautics research institutes: KTH, EPFL, IMFT, ICUBE, CERFACS, Univ. of Karlsruhe, ETH-Ecole Polytechnique de Zurich, among other. This consortium is coordinated by CFS Engineering in Lausanne, Switzerland. NSMB is a structured code that

includes a variety of efficient high-order numerical schemes and a considerable number of turbulence modelling closures in the context of LES, URANS and hybrid RANS-LES approaches. Since the initial consortium, Vos *et al.* (1998), NSMB highly evolved up to now and includes an ensemble of the most efficient CFD methods, as well as adapted fluid–structure coupling for moving and deformable structures. Nowadays the solver NSMB is mainly developed by the research institutes ICUBE in Strasbourg, IMFT in Toulouse, France and CFS Engineering. The code is also used by AIRBUS Aerospace department for hypersonic simulations as well as by RUAG Aerospace, EPFL in Switzerland and finally Technical University of Karlsruhe and TUM Munich in Germany. These developments can be found in Hoarau (2002) regarding URANS modelling for strongly detached flows, Martinat *et al.* (2008), in the area of moving body configurations, Barbut *et al.* (2010) and Grossi *et al.* (2014) for Detached Eddy Simulation. NSMB solves the compressible Navier–Stokes equations using a finite-volume formulation on multi-block structured grids in parallel.

In this work, a preconditioning method was selected based on the artificial compressibility in our compressible solver NSMB in the implicit dual time stepping method with Lower Upper Symmetric Gauss Seidel (LU-SGS). The y+ value provided by this grid is smaller than 0.5 in the whole near wall domain, thus ensuring an optimal behaviour of the near-wall turbulence modelling with the appropriate damping for the eddy viscosity adopting a modified damping function regarding the Chien's k-$\epsilon$ model, Jin and Braza (1994), according to the Organised Eddy Simulation (OES) approach, Bourguet *et al.* (2008). A study of the time step has been carried out for the 2D simulations. A $dt = 10^{-5}$ second was found to be sufficient after a detailed investigation and was able to better capture the physics for the morphing at high frequency vibrations. A typical number between 60 and 100 inner steps was sufficient for the convergence in the dual time process. A comparison of the numerical results of the pressure coefficients with the experimental results obtained from the IMFT wind tunnel (see figure 2) is presented in the figure 3.

Based on previous studies in our research group which examined the predictive ability of various turbulence models, Bourguet *et al.* (2008), Szubert *et al.* (2015) and Jin and Braza (1994), it was shown that the standard two-equation k-$\epsilon$ Chien model, Chien (1982) was not able to produce the main flow instabilities and the unsteadiness at the present values of incidence and Reynolds number. However, the Organised-Eddy Simulation (OES) model, Braza *et al.* (2006), Bourguet *et al.* (2008) provides quite well the dynamics of the flow detachment dynamics including the separated shear layers and the wake instabilities. Furthermore, the OES approach is not intrinsically 3D and provides quite a good evaluation of the main flow instabilities, thus allowing a rich parametric study of the morphing actuations before selecting a reduced number of cases for a 3D investigation. In the present study, this turbulence modelling approach has been used and shows a clear appearance of low frequency instabilities as the von Kármán vortices past the trailing edge on the two-element configuration involving a large gap between the main wing and the flap, these aspects are crucial for the modification of the flow dynamics and are well captured by the present approach. The refined grid has around 300 cells on the airfoil and the flap and minimum cell size less than 1 mm near the flap's trailing-edge to capture the detachment of the boundary layer near the trailing edge. This grid showed its ability to

capture the real flow modification in the wake region when the morphing is activated.
The experimental prototype consists of a high-lift A320 LS prototype with two elements presented in the figure 2, containing a wing and a flap. In the IMFT large subsonic wind tunnel S1, an aerodynamic evaluation has been investigated for two configurations (Clean and take-off) with several degrees of incidence and different Reynolds numbers in the range [1-4] Million. This wind tunnel is an Eiffel type, which consists of a cylindrical central building containing the experimental chamber, the assembly and modification workshop, as well as the measuring equipment. The section of the collector decreases gradually to a diameter of D = 2.40 m to the outlet. However, at the entrance the diameter is 6 m. This manifold is made of sheet steel 3 mm thick. The inlet section includes two filters in the desired weight to suppress the vortex movements of the air that must be without the operation of the blower. The diffuser consists of a frustoconical section of 11.50 m, with an apex angle slightly lower than $8^{\circ}$, an entrance diameter of 2.70 m. This wind tunnel has a contraction section upstream of the test section with a double level of honeycombs ensuring a low turbulence intensity of order 1 %, as well as end plates attenuating the extremity effects and ensuring a most uniform flow with low turbulence level, to provide uniform low turbulent flow.
Experimental and numerical results are provided in the figure 3 of the Pressure coefficient (CP) for the LS prototype at $0^{\circ}$ angle of attack and Reynolds number of $1\text{x}10^{6}$ in the clean configuration (the flap is attached to the wing). There is a difference of CP in the pressure depression located in the leading edge of the wing between the numerical simulations by the NSMB solver and the experimental results from the wind tunnel. The numerical approach is affected by the 2D approximation previously mentioned which was performed with farfield conditions and does not consider the confinement with the presence of the upper, lower and sided walls. In addition, in another previous study of Marouf *et al.* (2020) and Marouf *et al.* (2019), a comparison with published results of two-element airfoil-flap similar to the A320 prototype with 3D simulations with OES-DDES and SST-DDES showed a good approximation with 2D results.
More detailed experimental tests of unsteady pressure measurements were carried out in the wind tunnel and are provided by means of piezo resistive pressure transducer placed at 72% of the chord on the upper surface of the flap and near the trailing-edge in the takeoff position to capture the near wake instabilities (predominant frequencies). These results are discussed with those obtained by the numerical model. Power Spectral Density (PSD) of converged signals is computed for both cases. Converged experimental signal of 210 seconds is stored each $10^{-4}$ second (see figure 4b for the signal sample) and compared to a numerical signal of 2 seconds stored each $10^{-5}$ second in the figure 4a. The PSD in the figures 4c and 4d revealed the existence of several predominant frequencies ($f_1$, $f_1 + f_2$, $f_2$ and $f_3$) quite similar in both configurations. The frequency $f_1$ corresponds to the vK instability bump formed in the range of 10-30 Hz in the numerical PSD.

A similar bump formation is obtained in the experimental psd in the figure 4d. The frequency $f_1$ is near 15 Hz in both cases and the bump formation is due to the interaction with smaller-scale turbulent chaotic motion present at this high Reynolds number. Then, a predominant frequency $f_2$ is also found, corresponding to the coherent vortices shedding in the upper shear layer and to their interaction with the vK mode (highlighted by the

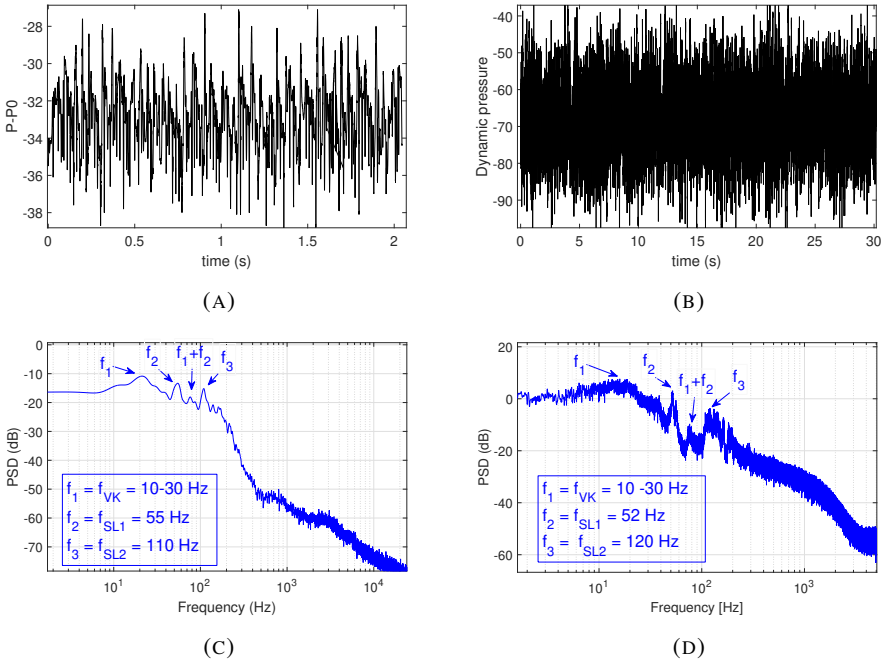


FIGURE 4: Pressure signal at 72% of the chord in the suction side of the flap. $(A)$ : numerical $\Delta P = P - P0$ , $(B)$ : experimental dynamic pressure (sensors). $(C)$ : PSD of the numerical signal. $(D)$ : PSD of the experimental signal

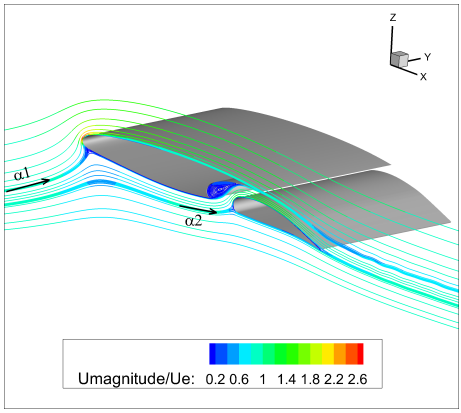


FIGURE 5: Streamlines around the Airbus A320 two-element wing-flap at the take-off position

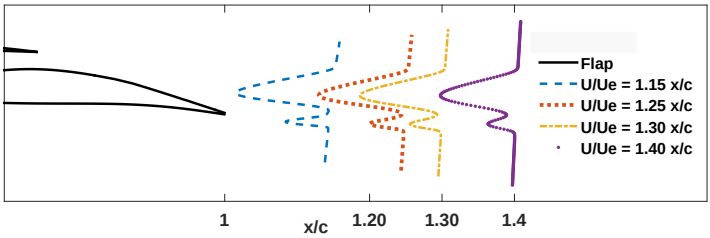


FIGURE 6: Mean non-dimensional streamflow velocity extracted from different position in the wake

streaklines in the next sections). The interaction between both instabilities generates new predominant frequencies as for example $f_1 + f_2$ found in the figures 4c and 4d. The predominant frequency $f_3$ is more associated to the lower shear layer and its smaller vortices in the formation region past the flap's trailing edge.
Furthermore, another comparison of these results can be made with a comparison of the study conducted by ( Jodin *et al.* (2017)) on the same prototype but in a smaller scale with a single element of chord $C$=0.7m at $Re$=0.5 million ($U$=10.5 m/s). It was found that the Strouhal number $St = 3$ ($fr = 46$ Hz) corresponds to the vK instability. The results of the Large-Scale prototype ($C = 2.72$m) at $Re$=2.25 million ($U$=12.47 m/s) are in good qualitative agreement with these results. The vK instabilities have a $St$ of 3.27 ($fr = 15$ Hz).

## 3. FLOW CHARACTERISTICS

The flow around the high-lift configuration is investigated numerically to understand the physics, the wake behavior and the reasons of the appearance of the turbulent instabilities during the take-off position. This could help us to find out an optimal morphing region with a specific vibration frequency at a certain deformation. The figure 5 presents the streamlines and highlights the alignment of flow with the lower surface of the airfoil. One distinguishes two angles of attack, $\alpha_1$ fixed from the initial condition and equal to 8° and $\alpha_2$ the new angle of attack with the flap formed by the modification of the flow due to the presence of the airfoil. Hence, a very small detachment of the boundary layer has been noticed due to the new modified angle of attack $\alpha_2$ with the flap. The flow around the two-element airfoil-flap can be decomposed into three different regions :

- Airfoil region : Starting from the airfoil and presenting a high axial velocity deficit in the near wake figure 6. The airfoil acts as a dominant bluff body in the flow at this angle of attack. The velocity deficit reaches critical values, which introduces the appearance of the wake instabilities.
- Flap region : Starting from the flap and presenting a smaller velocity deficit than the airfoil (figure 6) due to the presence of the airfoil.

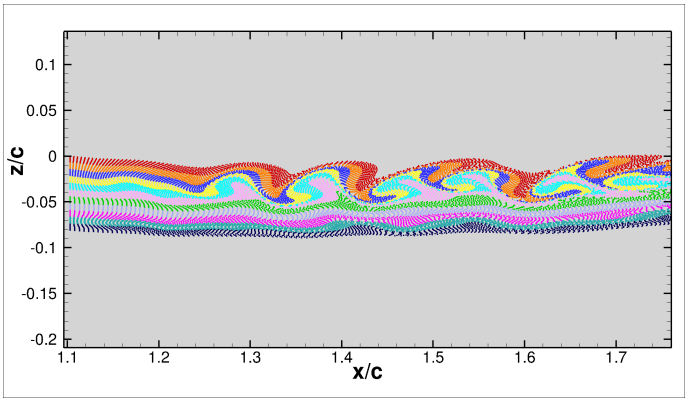


FIGURE 7: Visualisation of the wake instabilities by mean of streaklines in the static case (no vibration)

- Separating region : There is a considerable vertical distance between the airfoil and the flap in this region called the gap, which splits the velocity deficit into two parts (see figure 6). Consequently this separates the shearing of the airfoil and the flap in the wake. The C form at the end of the airfoil produces a recirculation region governed by an anticlockwise vortex.

There exists an interaction between these 3 regions in the wake and the flow in the wake is the result of a non-linear interaction between the lower and upper shear layers of the airfoil and the flap at this Reynolds number of $2.25\text{x}10^6$ and $8^\circ$ of angle of attack. The difference in the velocities between the upper and the lower shear layer is much higher in the airfoil's region than around the flap. This leads to creation of unstable waves which are amplified when they propagate further in the wake. Beyond critical state of the shearing mechanism, formation of vK vortices presented in figure 7 occurs from x/C=1.25 to x/C=1.8. These vortices are shed with a predominant frequency between 10 - 30 Hz (see figure 10 ) and are not fully formed. Further in the wake for x/C > 2 these shear layers produce the full formation of the von Kármán vortex street. Near the flap, small disturbances in the mixing layer create a wavy deformation but this does not roll up to create vK vortices because of a smaller velocity deficit.

## 4. MORPHING THROUGH NEAR-TRAILING-EDGE VIBRATION AND SLIGHT DEFORMATION

The trailing edge of the flap is deformed as a function of time in numerical simulations, according to the dynamics of MFC piezoactuators instrumented experimentally in the morphing prototypes of previously mentioned studies. The unsteady movement and the slight deformation of these patches are introduced in the numerical model in the same way as in the experiments by Jodin *et al.* (2017) and Scheller *et al.* (2015), by using Arbitrary Lagrangian Eulerian (ALE) method ( Donea *et al.* (1982)) and a second order polynomial equation similar to the MFC patches deformation.

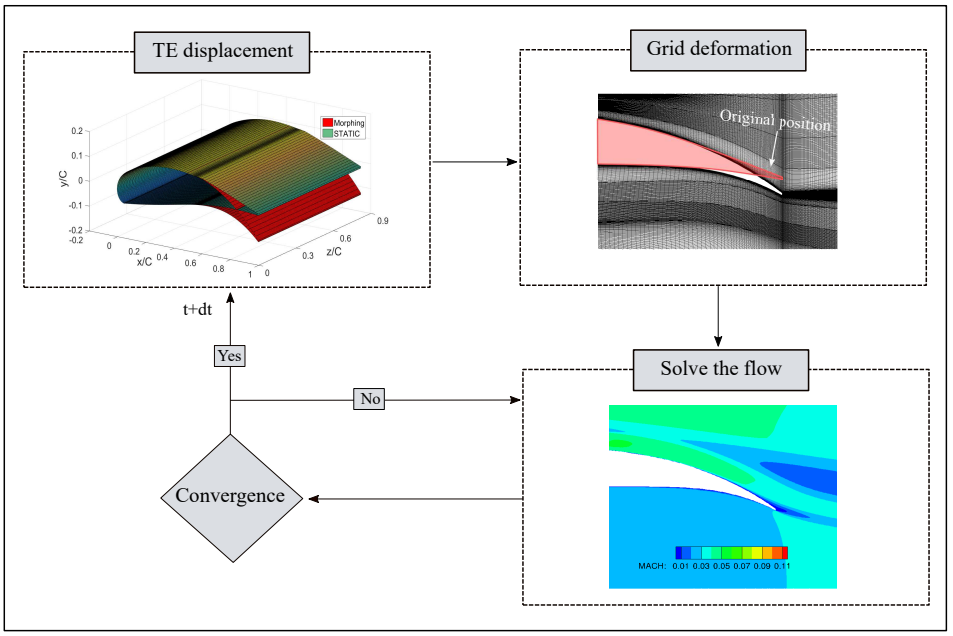


FIGURE 8: Dynamic grid deformation implemented in the NSMB solver to simulate the time-dependent morphing

The displacement of the flap geometry is imposed at first, then the new deformed grid is computed by means of Volume Spline Interpolation (VSI) and Trans-Finite Interpolation ( Guillaume *et al.* (2011)) remeshing methods. Next, the NSMB code solves the momentum equation and the pressure correction for the new grid in a convergence loop. Once the convergence is achieved, new time step $t + dt$ will be calculated as presented in the figure 8 . These methods are well adapted for small deformations to preserve good quality of the mesh as the orthogonality.

The frequency and amplitude values have been the object of a detailed parametric study as in the clean configuration in order to evaluate the morphing effects on the flow dynamics and the aerodynamic performances. The vibration of the flap introduces either an undulation in low frequency smaller than 200 Hz or a new anticlockwise vortex in the case where the frequency is higher as in figure 9. These morphing effects interact with the existing wake instabilities and modify the wake behavior. In order to understand the modification produced by the vibration, an area is selected close to the flap's trailing-edge and snapshots were saved for a time interval of $10^{-4}$ second to better analyze the effects of the dynamic morphing.

The angle of attack is more significant when the trailing-edge deformation is oriented to the pressure side. This configuration acts as a dominant bluff body. The air particles are submitted to an important shearing in the lower region past the trailing edge. At the same time, air particles located in the suction side of the trailing edge are dropped behind the trailing edge and split into two parts: the first creates a small recirculating vortex and the second part is mixed with the particles coming from the lower shear layer. This creates

new anticlockwise vortices which were not present in the static case, which have specific properties as an elliptic vortex shape with $(\beta, \alpha)$ parameters. The distance between two vortices corresponds to $L = U/(c.f_a)$, where $f_a$ is the actuation frequency. These new introduced vortices modify the flow further in the wake and affect the formation of the vK, thus producing an eddy-blocking effect ( Szubert *et al.* (2015)), resulting to a constriction of the shear layers and a thinning of the wake's width. The injected vortices are dissipated over 0.2 c, which will be analyzed in the next section.

### *4.1. Influence of the actuation frequency*

Several simulations are tested for the two-element airfoil-flap in the morphing configuration and compared to the static case (no vibration) taken as reference case. The purpose is to analyze the influence on the wake behavior, aerodynamic forces and energy distribution. A certain range of vibrations from low to high frequencies range of the order (30 Hz – 400Hz) at a fixed small deformation amplitude 0.35 mm were tested to show an optimal configuration allowing the attenuation or suppression of the wake instabilities and leading to an improved aerodynamic performance through the trailing-edge dynamic control. The frequency effects are visible in the wake. These effects from low to higher frequency ranges have been investigated in figure 10, which illustrate a streaklines visualization injected in different colored layers to reveal the exact modification of the flow. At a low frequency of 30 Hz in figure 10a, the shear layer instabilities are excited due to a resonance phenomenon produced by the morphing in the wake. The flap shear layer frequency is forced at 30 Hz vibration mode through the morphing and the natural frequency in the wake of the vK is between 30 Hz and 40 Hz. The anticlockwise vortices interact with the upper formed vK and expand them in the vertical direction. The actuation near to the natural frequency leads to a considerable amplification of the turbulent structures in the wake for the morphing compared to static configuration. Thus, the need to investigate frequencies of actuation $f_a$ greater than the natural frequency is important to analyze the wake response to higher vibration actuations. When the morphing frequency is in a medium range in the figure 10b (60 Hz) and figure 10c (100 Hz), this produces an undulation of the flap's shear layer, this has a direct effect on the vK and induces breakdown of the first vK vortex in into two smaller vK vortices for the 60 Hz actuation. In figure 10c the 100 Hz actuation shows an attenuation of the vK vortices from x/c = 1.2 to x/c = 1.4. The undulation interacts with the airfoil's shear-layer and prohibits the formation of the instabilities.

Higher frequencies are investigated up to 400 Hz. At 200 Hz, the undulation noticed in low frequency actuations is transformed to small anticlockwise vortices that were presented in the previous section (with a zoomed near trailing-edge area), this global view of the wake cannot exhibit them. The higher frequency have better effects than lower or medium frequencies. The figure 10d, 10e and 10f present respectively 200 Hz, 300 Hz and 400 Hz frequencies of actuation. A considerable attenuation of the vK vortices and the shear-layers instabilites occurs when the frequency actuation increases. In the figure 10e the 300 Hz frequency shows an optimal attenuation of these vortices and a complete disappearing of the instability from x/c=1.1 to x/c=1.7 compared to the static configuration.

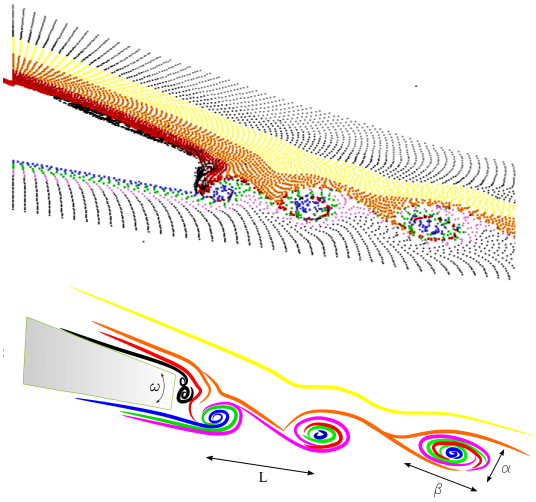


FIGURE 9: Zoom showing the near region of the flap's trailing-edge with colored streaklines visualisation and schematic description of high frequency morphing actuation at 300 Hz

The morphing injects and creates new vortices in the flow which are smaller and more energetic. These lasts interact with the upper and lower shear layers of the wing and prohibit the vK vortices to form. Above this optimal frequency, in the figure 10f the 400 Hz frequency gives again birth to these vortices. Consequently, a vibration at an optimal frequency suppresses and delays this kind of instabilities. This is related directly to a decrease of the predominant modes in the energy spectrum, which are the sources of the aerodynamic noise in the wake, as described in the frequency domain analysis detailed in the next section.

#### *4.1.1. Predominant wake frequencies*

To study the flow characteristics, a considerable number of snapshots has been saved each at a sampling rate of $10^{-3}$ second, to investigate the velocity signals at different positions in the near and farther wake. Monitor points in different specific coordinates at x/c = 0.95, x/c = 1.25 and x/c = 1.47 were stored for the static case and different morphing cases at high frequencies aiming to capture the motion of the low frequency instabilities like the vK existing in the wake and their modification due to the vibration. A Power Spectral Density (PSD) is computed for this monitor points signals by means of the Welch's weighted overlapped segment averaging estimator, using Hamming windows with 50 % overlap and zero padding ( Welch (1967)). Based on our research, this method shows the energy in a frequency domain and exhibits high energy modes related to the predominant instabilities created in the wake.

As previously analyzed, a natural predominant frequency $f_1$ in the range of 10 Hz to 30 Hz was noticed and corresponds to the vK vortex motion presented in figure 7. The

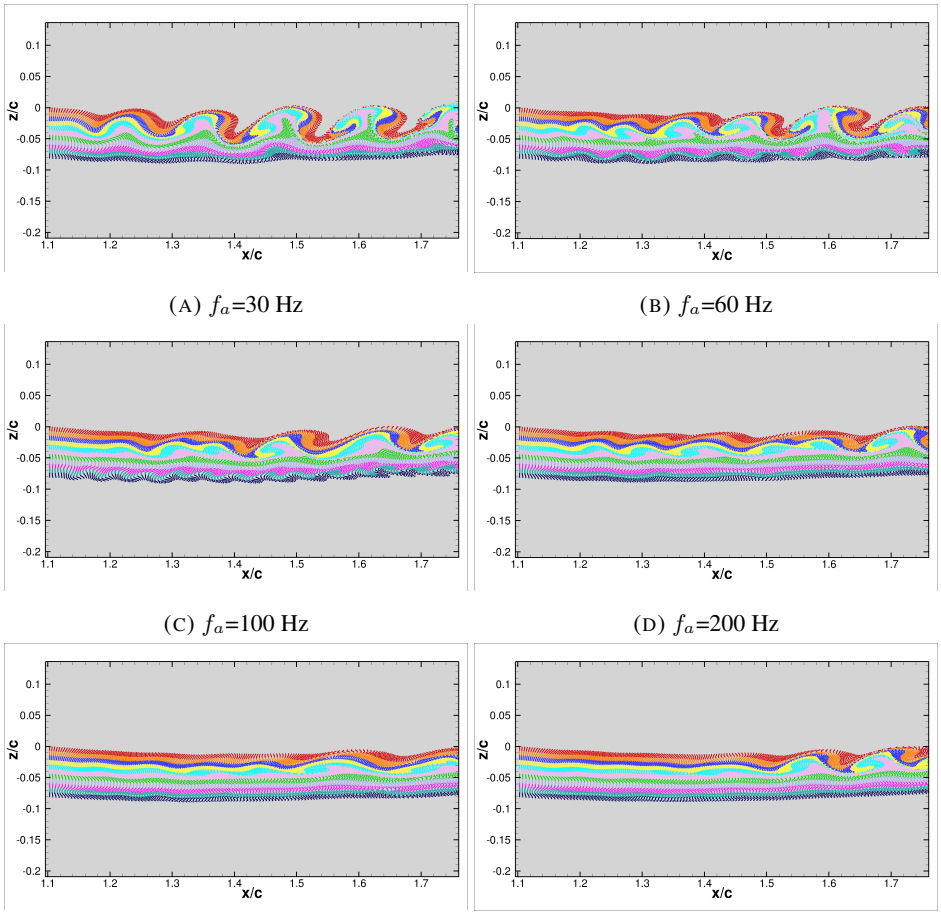


(A) $f_a$=30 Hz

(B) $f_a$=60 Hz

(C) $f_a$=100 Hz

(D) $f_a$=200 Hz

(E) $f_a$=300 Hz

(F) $f_a$=400 Hz

FIGURE 10: Streaklines visualisation for different actuation frequencies at a fixed slight deformation of 0.35mm

PSD method illustrates the principal bumps related to this instability and in addition it is followed by $f_2$ and $f_3$ corresponding to the shear-layers instabilities in the static case (see figure 11a). The morphing at high frequencies of 200 Hz, 300 Hz and 400 Hz with a low amplitude deformation, reveals a diminution of the vK and the shear-layers bumps of the predominant natural frequencies in the 3 positions in the figure 11a, 11b and 11c. Furthermore, some peaks at 200 Hz, 300 Hz and 400 Hz are visible and correspond to the frequencies of the trailing-edge actuation.

The morphing at higher frequency range introduces new smaller vortices which replace the existing instabilities by means of an eddy blocking effect and consequently generates a reduction and a delay in the formation of the vK vortices. Further in the wake at the position x/c = 1.47 in the figure 11c the vK vortices are fully developed and expanded to roll up into a von Kármán vortex street. Hence, the vibrations provide a considerable diminution of vK vortices frequency peaks compared to the static (no vibration) case.

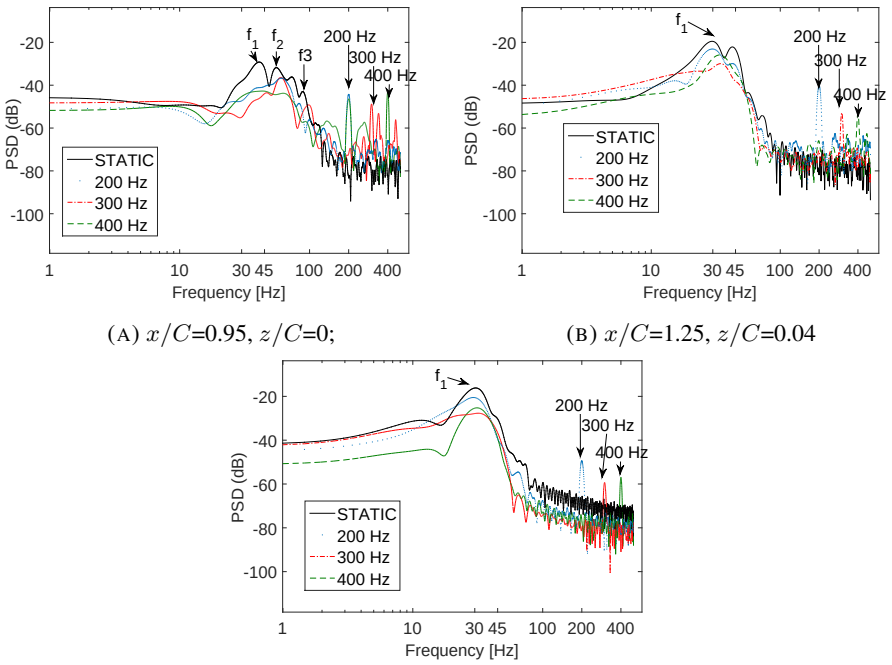


(A) $x/C$=0.95, $z/C$=0;

(B) $x/C$=1.25, $z/C$=0.04

(C) $x/C$=1.47, $z/C$ = 0.04

FIGURE 11: Power spectral density of the crossflow velocity for different high frequency actuation cases in the wake.

The 300 Hz case at a 0.35 mm amplitude of deformation causes a better decrease of the spectral energy peaks compared to 200 Hz and 400 Hz and can achieve between -10 dB to -15 dB related to the aerodynamic noise. These results match with those in figure 10, where the 300 Hz produces a complete disappearance of these instabilities better than the other frequencies and even further in the wake.

### *4.2. Influence of the amplitude*

The effects of the amplitude are investigated in this section. A matrix of amplitude frequency was necessary to draw the different effects of the trailing-edge morphing. A range of higher amplitudes compared to the previous case presented (with 0.35mm) has been selected with actuation frequencies from a lower to a higher range. The figure 12 illustrates the 3x3 matrix of amplitude-frequency, where amplitudes of 0.5 mm, 1 mm and 1.5 mm were chosen and frequencies of 60 Hz, 100 Hz and 300 Hz. As mentioned in the section 4, an undulation of the flap's shear-layer is created due to the morphing at lower frequencies than 200 Hz.

In the figure 12a, 12b and 12c at a fixed actuation of 60 Hz, when the morphing amplitude increases, the undulation in the flap's shear layer becomes higher and expands in the vertical and horizontal directions. On the other hand, the width of the vK vortices is diminished compared to the static case in the figure 7. Furthermore, in the figure 12d, 12e

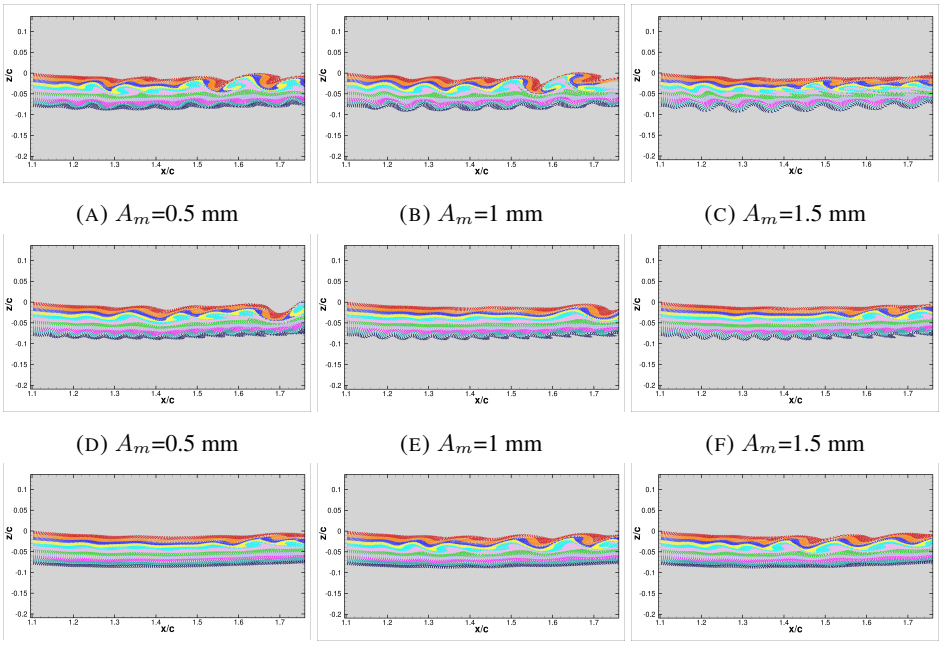

(A) $A_m$=0.5 mm (B) $A_m$=1 mm (C) $A_m$=1.5 mm

(D) $A_m$=0.5 mm (E) $A_m$=1 mm (F) $A_m$=1.5 mm

(G) $A_m$=0.5 mm (H) $A_m$=1 mm (I) $A_m$=1.5 mm

FIGURE 12: Streaklines visualisation for different actuation amplitudes and frequencies. $(A)$, $(B)$ and $(C)$ $f_a$=60 Hz; $(D)$, $(E)$ and $(F)$ $f_a$=100 Hz; $(G)$, $(H)$ and $(I)$ $f_a$=300 Hz

and 12g, when the frequency of actuation is fixed at 100 Hz, it appears that the undulation became smaller than the previous case due to a higher trailing-edge speed vibration. The vK vortices disappear in the near wake. This created undulation interacts with the airfoil's shear-layer where the vK vortices are formed, and as a consequence it prohibits their formation and expansion compared to the static case. This last is formed in the lower shear-layer and interacts with the upper Turbulent-Non-Turbulent (TNT) interface outside the Turbulent Boundary Layer (TBL) ( Szubert *et al.* (2015)). The undulation and the TNT interface enclose the vK vortices and decrease their width until they disappear. The morphing undulation dominates the vK vortices in the wake for a higher amplitude case and lower or medium frequencies such as 60 Hz and 100 Hz. However, contrary to the figure 12g, 12h and 12i when the frequency is set at 300 Hz, an increase of the amplitude more than 1 mm reveals the return of the formation of smaller vK vortices.
This investigation of frequency-amplitude helped to highlight where the morphing of the flap's trailing-edge has optimal configurations. One distinguishes the anti-diagonal matrix in the figure 12c, 12e and 12g are the best cases. As a result, low frequency-high amplitude, medium frequency-medium amplitude and high frequency-low amplitude are the most optimal configurations to suppress the wake instabilities.

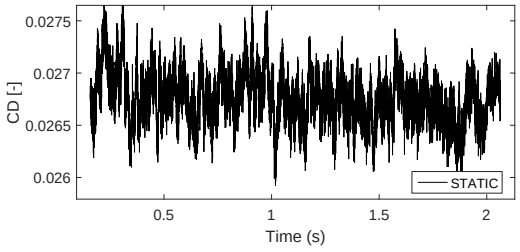


(A)

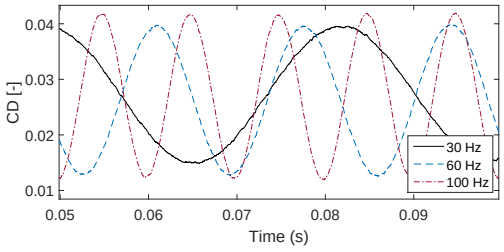


(B)

FIGURE 13: Time series of the drag coefficient. $(A)$ converged static case; $(B)$ morphing at different actuation frequencies

### *4.3. Effects of the morphing on the aerodynamic forces*

An investigation is carried out in order to analyze the morphing effects on the local aerodynamic loads over the wing-flap system. The simulations are performed at the same Reynolds number and angle of attack for the take-off position. The lift and drag forces are computed by means of an integration of the pressure and viscous forces over a wing-flap surfaces. To ensure the statistical convergence of the numerical simulations an acquisition time of 1 s is employed for 100 000 stored points in a converged signal. The figure 13a displays the drag coefficient signal from static (no vibration) configuration. The signal corresponds to a choatic regime due to the high Reynolds number. Irregular fluctuations are captured by the refined grid in the static case where the local minimum cell size is less than 1mm. However, the morphing in the figure 13b shows only sinusoidal harmonic actuation frequencies. When the flap's trailing-edge is vibrating at a certain fixed frequency, a lock-in phenomenon appears on the pressure signal and modifies the mean values of the drag and the lift forces. The morphing introduced either a new undulation or small vortices which replaces the existing instabilities, adds kinematic energy into the shear-layer which produces a breakdown of the low frequency instabilities and reduces the thickness of the wake, and consequently reduce the total drag. The vortex shedding loses its coherency due to the disorganization of the structures of the flow in the wake. Through the morphing, this mode is suppressed and replaced by a new mode, where the instabilities do not appear in the upper and lower shear-layers for high frequency actuations near to the trailing edge of the flap.

Compared to the static configuration, the injection of beneficial vortices influences

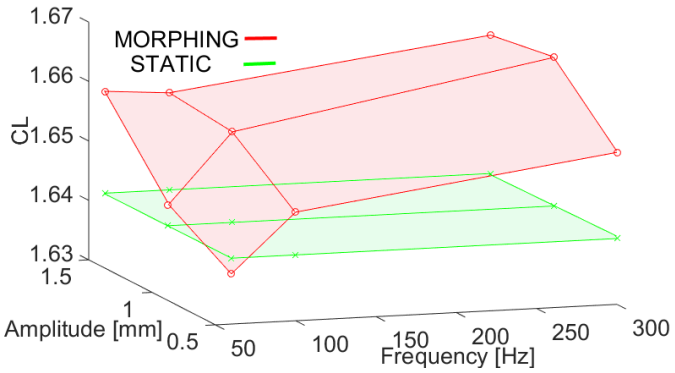


FIGURE 14: Mean lift coefficient at the take-off position in function of different actuation frequencies and amplitudes compared to the static case

the pressure distribution over the flap and even over the airfoil by means of feedback effect. The lift coefficient CL varies as function of the frequency in the range of (60 Hz – 300 Hz) and the amplitude actuation in a range of (0.5mm – 1.5mm) as presented in figure 14. The best CL is in the higher frequency/higher amplitude. The effect of high frequencies has already been discussed. The actuation at high amplitudes which means smaller cambering at 1.5 mm corresponds to an increase of the angle of attack of the flap's trailing edge. This can explain the lift increase. An increase of the signal amplitude has been also noticed together with a higher regularity of the signal's temporal evolution. Another significant effect is that the drag coefficient CD has a small increase when the frequency and amplitudes are higher. A thorough and more detailed investigation should be undertaken to find out the optimal area where the CL/CD ratio is improved.

## 5. CONCLUSION

This paper presents a numerical study of the morphing effects on the wake dynamics and the aerodynamic forces of an infinite A320 wing. Numerical data of the Large-Scale (LS) prototype of the SMS European project were validated with respect to experimental data in the clean and the take-off configurations for $Re = 1 \times 10^6$, $2.25 \times 10^6$ and angles of attack of $0°$, $8°$. Afterwards, the numerical configuration was set in the take-off position to investigate the morphing effects for a high-lift wing-flap configuration. An explanation of the flow around the wing-flap system and a wake analysis of the turbulent structures are provided. The morphing is then activated in the flap's trailing-edge actuating at high frequency vibration-low amplitude deformation. Effects of the dynamic vibration reveal a suppression and delaying of the vK vortices formation in the wake after a detailed investigation of a frequency and amplitude of actuation domains. In addition, an energy-frequency analysis showed a significant reduction of low frequencies instabilities and obtained approximately 15 dB of noise reduction in the predominant frequency peak. Finally, the dynamic morphing improves the aerodynamic lift compared to the classical

static system through a vortex breakdown of largest coherent structures and enhancement of good vortices.
In a next step, hybrid morphing is to be investigated by coupling a low frequency- high amplitude deformation called dynamic cambering and high frequency-low amplitude .

## References

Abdessemed, C. Yao, Y. Bouferrouk, A. Narayan, P. (2018), "Morphing airfoils analysis using dynamic meshing",*International Journal of Numerical Methods for Heat & Fluid Flow*, Vol. 28 No. 5, pp. 1117–1133,URL https://doi.org/10.1108/HFF-06-2017-0261.

Barbut, G., Braza, M., Hoarau, Y., Barakos, G., Sévrain, A. and Vos, J.B. (2010), "Prediction of Transonic Buffet around a Wing with Flap", in S.H. Peng, P. Doerffer and W. Haase, (Eds.) "Progress in Hybrid RANS-LES Modelling", Springer Berlin Heidelberg, Berlin, Heidelberg, pp. 191–204, URL https://doi.org/10.1007/978-3-642-14168-3_16.

Bourguet, R., Braza, M., Harran, G. and Akoury, R.E. (2008), "Anisotropic Organised Eddy Simulation for the prediction of non-equilibrium turbulent flows around bodies", *Journal of Fluids and Structures*, Vol. 24 No. 8, pp. 1240–1251, URL https://doi.org/10.1016/j.jfluidstructs.2008.07.004.

Braza, M., Faghani, D. and Persillon, H. (2001), "Successive stages and the role of natural vortex dislocations in three-dimensional wake transition", *Journal of Fluid Mechanics*, Vol. 439, pp. 1–41, URL 10.1017/S002211200100458X.

Braza, M., Perrin, R. and Hoarau, Y. (2006), "Turbulence properties in the cylinder wake at high Reynolds numbers", *Journal of Fluids and Structures*, Vol. 22 No. 6, pp. 757–771, URL https://doi.org/10.1016/j.jfluidstructs.2006.04.021.

Chien, K.Y. (1982), "Predictions of Channel and Boundary-Layer Flows with a Low-Reynolds-Number Turbulence Model", *AIAA Journal*, Vol. 20 No. 1, pp. 33–38, URL 10.2514/3.51043.

Chinaud, M., Rouchon, J.F., Duhayon, E., Scheller, J., Cazin, S., Marchal, M. and Braza, M. (2014), "Trailing-edge dynamics and morphing of a deformable flat plate at high Reynolds number by time-resolved PIV", *Journal of Fluids and Structures*, Vol. 47, pp. 41–54, URL https://doi.org/10.1016/j.jfluidstructs.2014.02.007.

Chinaud, M., Scheller, J., Rouchon, J.F., Duhayon, E. and Braza, M. (2013), "Hybrid Electroactive Wings Morphing for Aeronautic Applications", in "Mechatronic Systems and Materials IV", volume 198, Trans Tech Publications Ltd, pp. 200–205, URL 10.4028/www.scientific.net/SSP.198.200.

Donea, J., Giuliani, S. and Halleux, J.P. (1982), "An arbitrary lagrangian-eulerian finite element method for transient dynamic fluid-structure interactions", *Computer Methods in Applied Mechanics and Engineering*, Vol. 33 No. 1, pp. 689–723, URL https://doi.org/10.1016/0045-7825(82)90128-1.

Grossi, F., Braza, M. and Hoarau, Y. (2014), "Prediction of Transonic Buffet by Delayed Detached-Eddy Simulation", *AIAA Journal*, Vol. 52 No. 10, pp. 2300–2312, URL 10.2514/1.J052873.

Guillaume, M., Gehri, A., Stephani, P., Vos, J.B. and Mandanis, G. (2011), "F/A-18 vertical tail buffeting calculation using unsteady fluid structure interaction", *The Aeronautical Journal (1968)*, Vol. 115 No. 1167, pp. 285–294, URL 10.1017/S0001924000005777.

Hoarau, Y. (2002), "Analyse physique par simulation numérique et modélisation des écoulements décollés instationnaires autour de surfaces portantes", Thèse de doctorat dirigée par Braza, Marianna Dynamique des fluides .

Hoarau, Y., Braza, M., Ventikos, Y., Faghani, D. and Tzabiras, G. (2003), "Organized modes and the three-dimensional transition to turbulence in the incompressible flow around a NACA0012 wing", *Journal of Fluid Mechanics*, Vol. 496, pp. 63–72, URL 10.1017/S0022112003006530.

Hoarau, Y., Pena, D., Vos, J.B., Charbonnier, D., Gehri, A., Braza, M., Deloze, T. and Laurendeau, E. (2016), "Recent Developments of the Navier Stokes Multi Block (NSMB) CFD solver", in "54th AIAA Aerospace Sciences Meeting", URL 10.2514/6.2016-2056.

Jin, G. and Braza, M. (1994), "Two-equation turbulence model for unsteady separated flows around airfoils", *AIAA Journal*, Vol. 32 No. 11, pp. 2316–2320, URL 10.2514/3.12292.

Jodin, G., Motta, V., Scheller, J., Duhayon, E., Döll, C., Rouchon, J.F. and Braza, M. (2017), "Dynamics of a hybrid morphing wing with active open loop vibrating trailing edge by time-resolved PIV and force measures", *Journal of Fluids and Structures*, Vol. 74, pp. 263–290, URL https://doi.org/10.1016/j.jfluidstructs.2017.06.015.

Jodin, G., Tekap, Y.B., Saucray, J.M., Rouchon, J.F., Triantafyllou, M. and Braza, M. (2018), "Optimized design of real-scale A320 morphing high-lift flap with shape memory alloys and innovative skin", *Smart Materials and Structures*, Vol. 27 No. 11, p. 115005, URL 10.1088/1361-665x/aae2ef.

Lu, W., Tian, Y. and Liu, P. (2017), "Aerodynamic optimization and mechanism design of flexible variable camber trailing-edge flap", *Chinese Journal of Aeronautics*, Vol. 30 No. 3, pp. 988–1003, URL https://doi.org/10.1016/j.cja.2017.03.003.

Marouf, A., Hoarau, Y., Vos, J. B., Charbonnier, D., Bmegaptche Tekap, Y. and Braza M. (2019), "Evaluation of the aerodynamic performance increase thanks to a morphing A320 wing with high-lift flap by means of CFD Hi-Fi approaches", *AIAA Aviation 2019 Forum*, URL 10.2514/6.2019-2912.

Marouf A., Simiriotis N., Tô J.B., Bmegaptche Y., Hoarau Y., Braza M. (2020), "DDES and OES simulations of a morphing Airbus A320 wing and flap in different scales

at high Reynolds", in Hoarau Y., Peng SH., Schwamborn D., Revell A., Mockett C. "Progress in Hybrid RANS-LES Modelling. Notes on Numerical Fluid Mechanics and Multidisciplinary Design, vol 143. Springer, Cham", Springer Berlin Heidelberg (URL DOIhttps://doi.org/10.1007/978-3-030-27607-2_20.

Martinat, G., Braza, M., Hoarau, Y. and Harran, G. (2008), "Turbulence modelling of the flow past a pitching NACA0012 airfoil at 105 and 106 Reynolds numbers", *Journal of Fluids and Structures*, Vol. 24 No. 8, pp. 1294–1303, URL https://doi.org/10.1016/j.jfluidstructs.2008.08.002.

Scheller, J., Chinaud, M., Rouchon, J., Duhayon, E., Cazin, S., Marchal, M. and Braza, M. (2015), "Trailing-edge dynamics of a morphing NACA0012 aileron at high Reynolds number by high-speed PIV", *Journal of Fluids and Structures*, Vol. 55, pp. 42–51, URL https://doi.org/10.1016/j.jfluidstructs.2014.12.012.

Soulat, L., Pouangué, A.F. and Moreau, S. (2016), "A high-order sensitivity method for multi-element high-lift device optimization", *Computers & Fluids*, Vol. 124, pp. 105–116, URL https://doi.org/10.1016/j.compfluid.2015.10.013.

Szubert, D., Grossi, F., Garcia, A.J., Hoarau, Y., Hunt, J.C.R. and Braza, M. (2015), "Shock-vortex shear-layer interaction in the transonic flow around a supercritical airfoil at high Reynolds number in buffet conditions", *Journal of Fluids and Structures*, Vol. 55, pp. 276–302, URL doi.org/10.1016/j.jfluidstructs.2015.03.005.

Vos, J., Rizzi, A., Corjon, A., Chaput, E. and Soinne, E. (1998), "Recent advances in aerodynamics inside the NSMB (Navier Stokes Multi Block) consortium", in "36th AIAA Aerospace Sciences Meeting and Exhibit", URL 10.2514/6.1998-225.

Welch, P. (1967), "The use of fast Fourier transform for the estimation of power spectra: A method based on time averaging over short, modified periodograms", *IEEE Transactions on Audio and Electroacoustics*, Vol. 15 No. 2, pp. 70–73, URL 10.1109/TAU.1967.1161901.